

Thermo-Mechanical Model of Solidification Processes with Abaqus

Seid Koric and Brian G. Thomas

*National Center for Supercomputing Applications-NCSA &
Mechanical Science and Engineering Department
University of Illinois at Urbana-Champaign
1205 W. Clark Street
Urbana, IL 61801*

A computational thermo-mechanical model has been developed to simulate the continuous casting of shaped sections, such as used for thin steel slabs. A general form of the transient heat equation including latent-heat from phase transformations such as solidification and other temperature-dependent properties is solved numerically for the temperature field history. The resulting thermal stresses are solved by integrating the highly nonlinear thermo-elastic-viscoplastic constitutive equations using a two-level method. The procedure has been implemented into Abaqus, (Abaqus Inc., 2005) using a user-defined subroutine (UMAT) to integrate the constitutive equations at the local level (Koric, 2006). The model is validated both with a semi-analytical solution from Weiner and Boley (Weiner, 1963) as well as with an in-house finite element code CON2D (Li, 2004, Zhu, 1993) specialized in thermo-mechanical modeling of continuous casting. The model is applied to simulate a 3D segment of the solidifying steel shell as it moves down through a thin slab caster with a funnel mold, known for its complex geometry, using realistic operating conditions and temperature-dependant properties. It has provided valuable new insights into the complex dynamic 3D mechanical state of stress experienced by the solidifying shell due to the funnel geometry.

KEY WORDS: *Material Processing, Continuous Casting, Finite Elements, Abaqus, UMAT, CON2D, Fixed Grid, Solidification, Thin Slab Casting, Funnel Mold.*

1. Introduction and Previous Work

Many manufacturing and fabrication processes such as foundry shape casting, continuous casting and welding have common solidification phenomena. Probably one of the most important and complex among them is continuous casting. In fact most of the steel made today is produced through continuous casting. Even though the quality of the continuous casting is constantly improving, there is still a significant amount of work needed to minimize the amount of defects and to maximize the productivity. Some of the more important issues that influence the productivity and the quality of steel produced by the continuous casting process, are: uneven shell growth that influences the size of interfacial gap and the gap heat flow, leading to locally hot and thin parts of shell which can be another cause of longitudinal cracks and breakouts and transverse strains due to ferrostatic pressure from the liquid phase applied to a newly solidified shell can cause longitudinal cracks and breakouts.

Most of these phenomena occur during the early stages of solidification in the mold. Accurate determination of temperature, deformation and stress distributions during this time is important for correct prediction of surface shape and cracking problems in processes such as the continuous casting of steel.

The high cost of plant experiments under the harsh operating steel plant conditions makes it appropriate to use all available methods in simulating, optimizing, and designing this process. Even though physical modeling (experiment) of initial solidification has been conducted (Mizukama, 1999), the complexity of this process and phenomena that governs it make it difficult to model.

At the same time the increasing power of computers and development of numerical methods in last 25 years has helped researchers to better understand the governing principles of various material processing operations. The continuous casting process is not exception, and it has been subjected to more numerical models than any other process. However, it is a challenging task too, and there is large number of

computational difficulties encountered with numerical modeling of thermo-mechanical behavior of the shell in continuous casting.

In 1963, Weiner and Boley (Weiner, 1996) derived a semi-analytical solution for the thermal stresses arising during the solidification of a semi infinite plate. Although that work oversimplifies the complex physical phenomena of solidification, it has become a useful benchmark problem for the verification of numerical models (Zhu, 1993, Li, 2004, Koric, 2006). The constitutive models used in previous work to investigate thermal stresses during continuous casting first adopted simple elastic-plastic laws (Weiner 1963, Grill, 1976, Wimmer, 1996). Later, separate creep laws were added (Rammerstrofer, 1979, Kristiansson, 1984). With the rapid advance of computer hardware, more computationally challenging elastic-viscoplastic models have been used (Zhu 1993, Boehmer 1998, Farup, 2000, Li, 2004, Risso, 2006, and Koric, 2006) which treat the phenomena of creep and plasticity together since only the combined effect is measurable. While Lagrangian description of this process with fixed mesh is mostly adopted due to its easy implementation, an alternative mechanical model based on Eulerian-Lagrangian description has been proposed lately (Risso 2006). Similarly, the integration of viscoplastic laws ranges from easy-to-implement explicit methods (Morgan, 1978, Lewis, 1996), to robust but complex implicitly based algorithms (Zhu, 1993, Li, 2004, Koric, 2006).

It is a considerable challenge to implement the unified approach of these previous in-house models into a full scale FE analysis, and including other important phenomena such as contact. Such analysis would enable correct reproduction of the true 3D mechanical state in casting processes with complex geometry or with complex loading conditions. On the other hand, the easy-to-use commercial finite-element packages are now fully capable of handling 2D and 3D problems, having rich element libraries, fully imbedded pre and post processing capabilities, advanced modeling features such as contact algorithms, and can take full advantage of parallel-computing capabilities.

The work of Koric et al (Koric, 2006, Koric, 2007) implemented a robust local viscoplastic integration schemes from an in-house code CON2D (Zhu, 1993, Li 2004) into the commercial finite element package Abaqus via its user defined material subroutine UMAT including the special treatment of liquid/mushy zone. This opened the door for or realistic computational modeling of complex solidification processes with Abaqus.

2. Thermal Governing Equations

By using the uncoupled procedure (Abaqus Inc., 2005), Abaqus solves thermal equation first and the resulting temperature solution is used in the subsequent mechanical analysis. The local form of the transient energy equation is given in equation 1, (Lewis, 1996).

$$\rho \left(\frac{\partial H(T)}{\partial t} \right) = \nabla \cdot (k(T) \nabla T) \quad (1)$$

along with boundary conditions:

$$\begin{aligned} \text{Prescribed temperature on } A_T & T = \hat{T}(\mathbf{x}, t) \\ \text{Prescribed surface flux on } A_q & (-k \nabla T) \cdot \mathbf{n} = \hat{q}(\mathbf{x}, t) \\ \text{Surface convection on } A_h & (-k \nabla T) \cdot \mathbf{n} = h(T - T_\infty) \end{aligned} \quad (1a)$$

Where ρ is density, k is isotropic temperature dependant conductivity, H is temperature dependant enthalpy, which includes the latent heat of solidification. \hat{T} is a fixed temperature at the boundary A_T , \hat{q} is prescribed heat flux at the boundary A_q , h is film convection coefficient prescribed at the boundary A_h where T_∞ is the ambient temperature, and \mathbf{n} is the unit normal vector of the surface of the domain.

3. Mechanical Governing Equations

Solidification involves small strain, so the assumption of small strain is adopted in this work. The thermal strains which dominate thermo-mechanical behavior during solidification are on the order of only a few percent, or cracks will form (Thomas, 1986). Several previous solidification models (Kristansson, 1984, Zhu, 1993, Li, 2004, Risso, 2006) confirm that the solidified metal part indeed undergoes only small deformation during initial solidification in the mold. The displacement spatial gradient $\nabla \mathbf{u} = \partial \mathbf{u} / \partial \mathbf{x}$ is small so $\nabla \mathbf{u} : \nabla \mathbf{u} \approx 1$ and the linearized strain tensor is thus (Mase, 1999):

$$\boldsymbol{\varepsilon} = \frac{1}{2} [\nabla \mathbf{u} + (\nabla \mathbf{u})^T] \quad (2)$$

Then, the small strain formulation can be used, where Cauchy stress tensor is identified with the nominal stress tensor $\boldsymbol{\sigma}$, and \mathbf{b} is the body force density with respect to initial configuration.

$$\nabla \cdot \boldsymbol{\sigma}(\mathbf{x}) + \mathbf{b} = 0 \quad (3)$$

The boundary conditions are:

$$\begin{aligned} \mathbf{u} &= \hat{\mathbf{u}} \quad \text{on } A_u \\ \boldsymbol{\sigma} \cdot \mathbf{n} &= \Phi \quad \text{on } A_\Phi \end{aligned} \quad (3a)$$

where prescribed displacements $\hat{\mathbf{u}}$ on boundary surface portion A_u , and boundary surface tractions Φ on portion A_Φ define a quasi-static boundary value problem. The rate representation of total strain in this elastic-viscoplastic model is given by:

$$\dot{\boldsymbol{\varepsilon}} = \dot{\boldsymbol{\varepsilon}}_{el} + \dot{\boldsymbol{\varepsilon}}_{ie} + \dot{\boldsymbol{\varepsilon}}_{th} \quad (4)$$

where $\dot{\boldsymbol{\varepsilon}}_{el}, \dot{\boldsymbol{\varepsilon}}_{ie}, \dot{\boldsymbol{\varepsilon}}_{th}$ are the elastic, inelastic (plastic + creep), and thermal strain rate tensors respectively. Stress rate $\dot{\boldsymbol{\sigma}}$ depends on elastic strain rate, and in this case of linear isotropic material and negligible large rotations, it is given by equation 5 in which “:” represents inner tensor product.

$$\dot{\boldsymbol{\sigma}} = \underline{\underline{\mathbf{D}}} : (\dot{\boldsymbol{\varepsilon}} - \dot{\boldsymbol{\varepsilon}}_{ie} - \dot{\boldsymbol{\varepsilon}}_{th}) \quad (5)$$

$\underline{\underline{\mathbf{D}}}$ is the fourth order isotropic elasticity tensor given by equation 6.

$$\underline{\underline{\mathbf{D}}} = 2\mu \underline{\underline{\mathbf{I}}} + (k_B - \frac{2}{3}\mu) \mathbf{I} \otimes \mathbf{I} \quad (6)$$

Here μ, k_B are the shear modulus and bulk modulus respectively and are in general functions of temperature, while $\underline{\underline{\mathbf{I}}}, \mathbf{I}$ are fourth and second order identity tensors and “ \otimes ” is the notation for outer tensor product.

3.1 Inelastic Strain

Inelastic strain includes both strain-rate independent plasticity and time dependant creep. Creep is significant at the high temperatures of the solidification processes and is indistinguishable from plastic strain (Li, 2004). The inelastic strain-rate is defined here with a unified formulation using a single internal variable (Anand, 1982, Lush 1989), equivalent inelastic strain $\bar{\epsilon}_{ie}$ to characterize the microstructure. For steel solidification considered here, the equivalent inelastic strain-rate $\dot{\bar{\epsilon}}_{ie}$ is a function of equivalent stress $\bar{\sigma}$, temperature T , equivalent inelastic strain $\bar{\epsilon}_{ie}$, and steel grade defined by its carbon content %C.

$$\dot{\bar{\epsilon}}_{ie} = f(\bar{\sigma}, T, \bar{\epsilon}_{ie}, \%C) \quad (7)$$

$$\bar{\sigma} = \sqrt{\frac{3}{2} \sigma'_{ij} \sigma'_{ij}} \quad (8)$$

σ' is a deviatoric stress tensor defined in equation 9.

$$\sigma'_{ij} = \sigma_{ij} - \frac{1}{3} \sigma_{kk} \delta_{ij} \quad (9)$$

The mild carbon steels treated in this work are assumed to harden isotropically, so the von Mises loading surface, associated plasticity, and normality hypothesis in the Prandtl-Reuss flow law is applied (Mendelson 1983):

$$(\dot{\epsilon}_{ie})_{ij} = \frac{3}{2} \frac{\dot{\bar{\epsilon}}_{ie}}{\bar{\sigma}} \sigma'_{ij} \quad (10)$$

3.2 Thermal Strain

Thermal strains arise due to volume changes caused by both temperature differences and phase transformations, including solidification and solid-state phase changes between crystal structures, such as austenite and ferrite.

$$(\epsilon_{th})_{ij} = \int_{T_0}^T \alpha(T) dT \delta_{ij} \quad (11)$$

where α is temperature dependant coefficient of thermal expansion, and T_0 is the reference temperature and δ_{ij} is Kronecker's delta.

4. Local Time Integration of the Inelastic Constitutive Model implemented in UMAT

Owing to the highly strain dependant inelastic responses, a robust integration scheme is required to solve this system over a generic time increment Δt . The system of ordinary differential equations defined at each material point are converted into two "integrated" scalar equations and solved using special bounded Newton-Raphson method (Lush, 1989, Zhu, 1993, Koric, 2006). Details of this local bounded Newton Raphson scheme can be found at (Lush, 1989, Zhu, 1993, Koric, 2006) along with the derivation of the Jacobian consistent with this integration scheme.

The solution obtained from this “local” integration step from all material (gauss) points is used to update the global finite element equilibrium equation and solved using the Abaqus nonlinear finite element procedure (Abaqus Inc, 2005).

4.1. Treatment of Liquid/Mushy Zone

The great variation in material properties between liquid, mush, and solid creates significant numerical challenge to accurate thermo-mechanical simulations. In the current model the elements containing both liquid and solid are generally given no special treatment regarding either material properties or finite element assembly. The only difference is to choose an isotropic elastic-perfectly-plastic rate-independent constitutive model that enforces negligible liquid strength when the temperature is above the solidus temperature. This simple fixed-grid approach avoids difficulties of adaptive meshing or “giving birth” to solid elements. The yield stress $\sigma_Y = 0.01 \text{MPa}$ is chosen small enough to effectively eliminate stresses in the liquid-mushy zones, but also large enough to avoid computational difficulties. These liquid/mushy elements are evaluated using the standard radial-return algorithm, which is a special form of backward-Euler procedure (Crisfield, 1991, Zienkiewicz, 1991).

5. Numerical Validation

The solidification stress model used in this work was validated by comparison with a semi-analytical solution of thermal stress in an unconstrained solidifying plate, derived by Weiner and Boley (Weiner, 1963) and with a previous finite-element model, CON2D (Zhu, 1993, Li, 2004). Taking advantage of the large length and width of the test-problem casting, a one-dimensional solution with the generalized plane strain condition in both the y and z directions can produce the complete 3-D stress and strain state.

The domain adopted for this problem moves with the strand in a Lagrangian frame of reference as shown in Fig. 1. The domain consists of a thin slice through the plate thickness using 2-D generalized plane strain elements (in the axial z direction). In addition, a second generalized plane strain condition was imposed in the y-direction (parallel to the surface) by coupling the displacements of all nodes along the bottom edge of the slice domain.

The material in this problem has elastic-perfectly plastic constitutive behavior. The yield stress drops linearly with temperature from 20 MPa at 1000°C to zero at the solidus temperature 1494.4°C, which was approximated by $\sigma_Y = 0.03 \text{MPa}$ at the solidus temperature. A very narrow mushy region, 0.1°C, is used to approximate the single melting temperature assumed by Weiner and Boley

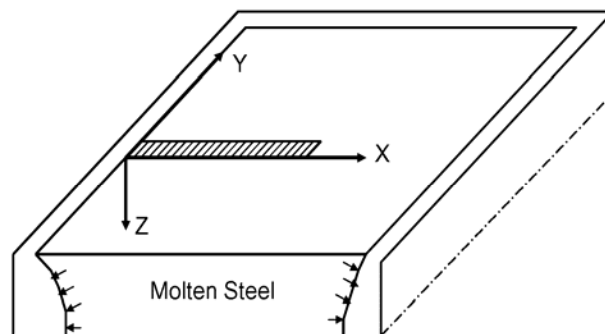
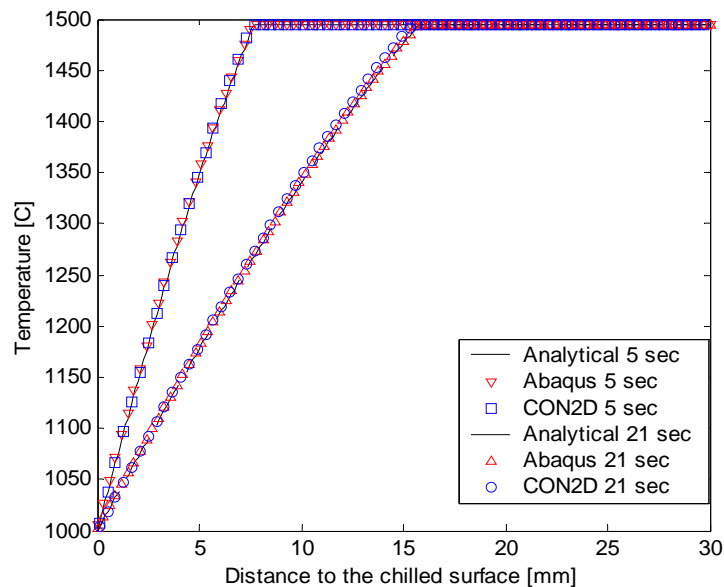


Figure 1. Solidifying Slice

Table 1. Constants used in solidification test problem.

| | |
|---|---------------------|
| Conductivity [W/mK] | 33.0 |
| Specific Heat [J/kg K] | 661.0 |
| Elastic Modulus in Solid [GPa] | 40.0 |
| Elastic Modulus in Liquid [GPa] | 14.0 |
| Thermal Linear Expansion Coefficient [1/K] | 0.00002 |
| Density [kg/m ³] | 7500. |
| Poisson's Ratio | 0.3 |
| Liquidus Temperature [°C] | 1494.45 |
| Fusion Temperature (analytical) [°C] | 1494.4 |
| Solidus Temperature [°C] | 1494.35 |
| Initial Temperature [°C] | 1495.0 |
| Latent Heat [J/kg K] | 272000.0 |
| Reciprocal of Liquid viscosity [MPa ⁻¹ sec ⁻¹] | 1.5x10 ⁸ |
| Surface Film coefficient [W/m ² K] | 250,000 |

Figures 2 and 3 show the temperature and the stress distribution across the solidifying shell at two different solidification times. The semi-analytical solutions were computed with MATLAB by C. Li et. al (Li, 2004). These figures also include the solution from an in-house code, CON2D (Zhu, 1993, Li, 2004) to this problem. Further comparisons of with CON2D for two-dimensional test problems also produced reasonable agreement. More details about this model validation can be found elsewhere (Koric, 2006) including comparisons with other less-efficient integration methods and a convergence study.

**Figure 2. Temperature distribution along the solidifying slice.**

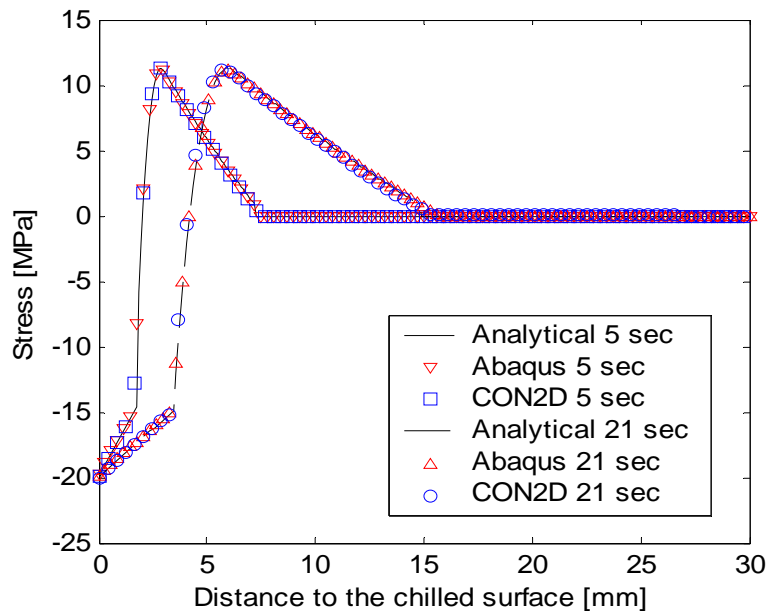


Figure 3. Y and Z Stress Distributions along the solidifying slice.

6. Thermo-Mechanical Model of Thin Slab Casting

Thin slab casting was first introduced in 1986 in Nucor Steel's plant in Crawfordsville Indiana. This technology features casting of about 50-mm thick slabs, which are 1/3 thinner than conventional cold cast rolled slab. Thermo-mechanical modeling of thin slab casting has received much less attention than conventional thick casting. The main additional modeling complication comes from the computational difficulty faced when modeling transient geometry of the funnel shape as the strand domain travels in the mold. A. Cristallini et al. (Cristallini, 1999) developed a two-dimensional transient thermal and stress analysis assuming elastic-plastic behavior of shell to design new funnel geometry. Park et al. (Park, 2002) implemented a 2D generalized plain strain approach with elastic-viscoplastic constitutive model by imposing a severe taper in the funnel area to emulate the slope of the funnel that pushes the strand. While this approach was able to predict temperature and transverse stress results, the axial stresses in the casting direction, which likely are responsible for internal transverse cracks, can only be calculated properly with a 3D model that has some thickness in the casting direction. A novel 3D thermo-mechanical analysis of a thin slab casting is performed with our Abaqus model with UMAT on the latest parallel computing platforms.

6.1 Geometry and FE Model

Fig. 4 shows a schematic of thin slab casting (Kowaski Steel, 1999). Aside from a thinner mold width than conventional thick caster, one additional significant difference is a funnel shape section across its central upper part. This design provides sufficient space for the introduction of a large size bifurcated submerged entry nozzle. The rest of the wide mold faces out of funnel region stays straight and parallel like any other rectangular mold. The funnel section narrows down gradually into a rectangular cross section which gives the final shape to the slab casts.

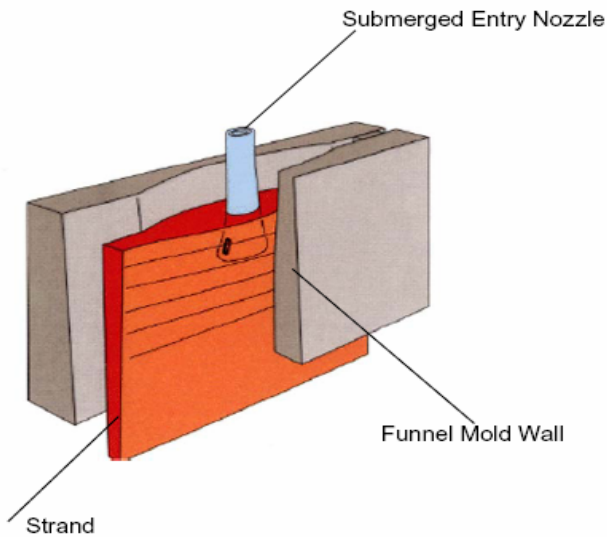


Figure 4. 3D Schematic of thin slab casting.

Fig. 5 has geometry of a thin mold used in this work. Generally, the shape of funnel can be characterized by the width and depth of funnel. The total width of the funnel is 750 mm consisting of two bends. The inside concave funnel bend is 400 mm wide where there is an inflection point that changes funnel curvature from concave to convex., the rest of the funnel is a convex outside bend. At the lower part of mold the wide faces at the funnel region becomes almost parallel, ie. the funnel depth tapers away linearly from 40 mm at the top of the mold to 6 mm at 900 mm down from the mold top. The meniscus plane is 100 mm lower than the mold top so that working mold length is 1100 mm. The slab thickness varies for the center of the funnel from 170 mm at mold top to 108 mm at mold exit, for the concave/convex inflection point from 148 mm at mold top to 93.1 at mold exit, and stays the same at 90 mm for the straight part of the mold.

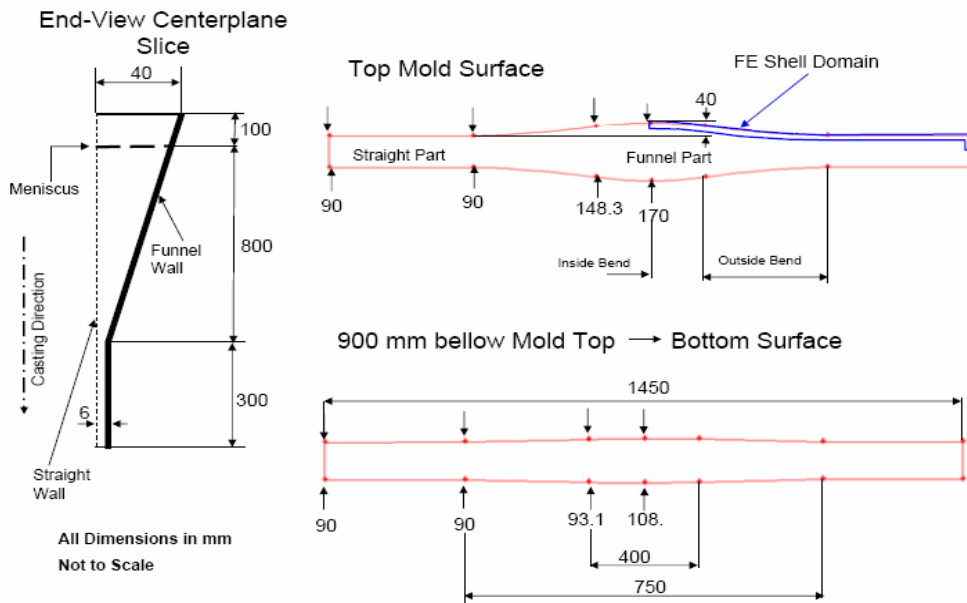


Figure 5. Geometry of a thin slab casting mold.

One quarter of the mold and the strand in it is modeled. The liquid domain is highly reduced to save cpu time and to reduce possible convergence problems in the volatile liquid/mushy region. Unlike any other 2D models, this FE model has a thickness of 100 mm in the casting direction; see Fig 6 of the 3D FE domain viewed from the bottom of the mold. The usual symmetry BC-s are enforced on the central planes normal to the wide and narrow faces. In addition, the symmetry BC in the axial direction z is enforced on the bottom surfaces of the mold and strand.

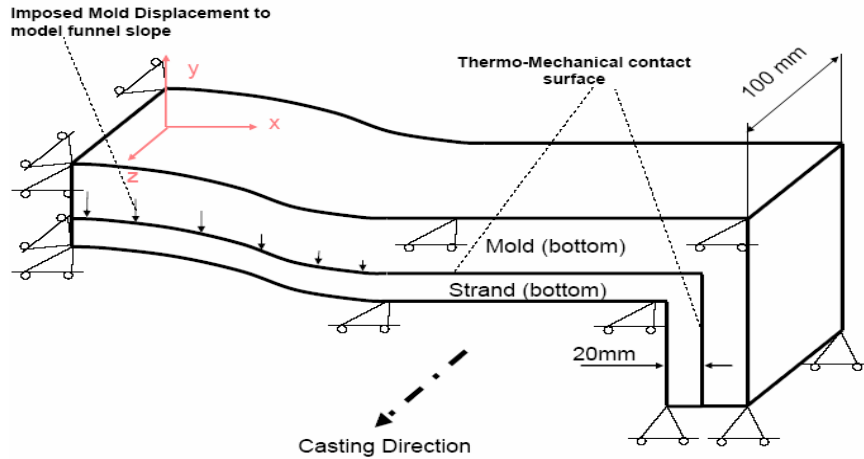


Figure 6. 3D Model and BC-s.

Due to the axial movement of 3D domain in Lagrangian frame of reference, the different material points and nodes in axial direction have different local times. Equation 12 is used to calculate the local time that a material point spends in the mold.

$$t_{\text{local}} = \frac{L_z}{\frac{v_c}{60}} \left(\frac{Z}{L_z} - 1 \right) + t_{\text{ref}} \quad (12)$$

where L_z is the domain thickness of 0.1 m in the casting direction, v_c is the casting velocity of 3.6 m/min, Z is the axial coordinate of a material point in the local coordinate system sitting on the top plane and traveling with the domain, and t_{ref} is the time of the reference plane which is chosen to be the bottom plane and is the time that Abaqus passes to UMAT.

The strand material is 0.21%C steel with temperature dependant properties which includes: conductivity, specific heat, enthalpy, elastic modulus, and thermal expansion coefficient (Li, 2004, Koric, 2006). The specific form of the inelastic law form from equation 7 is Kozlowski III law (Kozlowski, 1992) for austenite steels. The transient heat transfer analysis is first run for the strand domain to calculate its spatial and temporal temperature fields. The thermal boundary condition at the shell surface is modeled by use of a heat flux which is obtained from the plant measurements down the mold (Park, 2002). This flux data is curve fitted and prescribed as a function of the local time bellow meniscus in Fig. 7. The previous work (Li, 2004, Koric, 2007) revealed the formation of air gaps in the mold/shell interface in the corner region due to 2D heat flow corner effects. Therefore in order to account for the expected gap formation and thus avoid corner overcooling, the heat flux profile is reduced to 60% of its nominal value. This reduction is applied linearly starting 20mm from the corner on both wide and narrow strand surfaces. Fig. 7 also shows this reduced flux curve imposed at the corner.

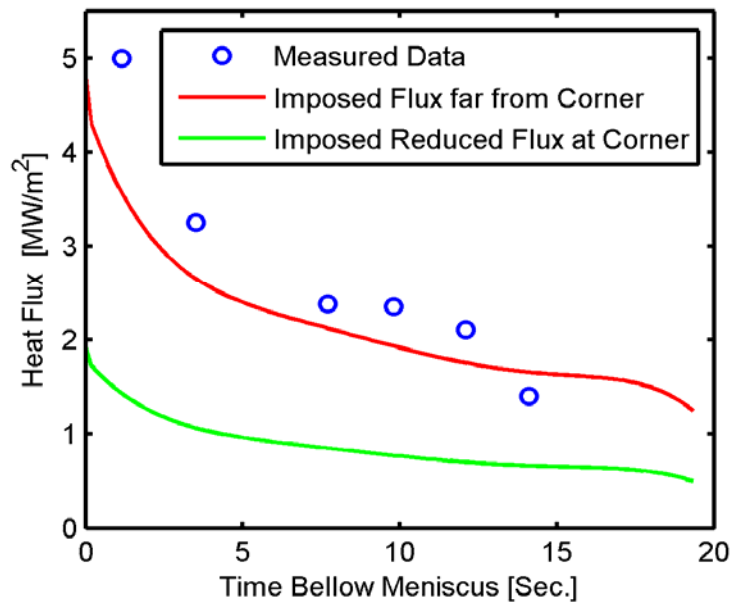


Figure 7. Imposed heat flux BC

The result temperature file is used for a subsequent stress analysis. The mechanical contact between 3D surfaces of the shell and the mold wall is modeled with Abaqus softened contact capabilities (Abaqus Inc., 2005). Ferrostatic pressure is modeled by means of DLOAD subroutine linearly increasing with respect to the local time for each material point on the shell surface pulled towards the mold wall. The funnel taper is modeled with the imposed displacement history to the funnel mold contact nodes by means of DISP subroutine. The total displacement is calculated from the difference between the funnel mold surface profiles at the top and the bottom of the mold for a few points along the funnel mold surface. This displacement data is curve fitted with the third order polynomial to yield the x directional (transverse) dependence. Finally this displacement function is linearly scaled with respect to the local total time bellow the meniscus.

The domain is meshed with 8-node brick elements (Abaqus Inc., 2005) with the total number of degrees of freedom close to 500,000. Abaqus 6.5 was run in parallel using the SMP direct solver with 4 cpus on the NCSA's AMD 64 cluster.

6.2 Results

Fig. 8 has a detail corner bottom shell surface distortion in the mold with the corner gap formed at 12 sec with temperature contour imposed. Since this model does not have mold taper modeled, the real shell would not probably form such a big gap, if the taper of the narrow face was put into the simulation.

Temperature contour is given in Fig. 9 at 19 sec., ie. when the bottom domain is exiting mold. Parallel isotherms normal to the casting direction confirm validity of the assumption used in all 2D cases that heat conduction in casting direction is negligible. Complicated geometry of the funnel region does not seem to produce any unexpected temperature results. Most of the shell surface is still cooling uniformly with respect to the local time it spends in the mold except in the corner and a small spot where funnel turns into straight part. Even though there is a drop of heat extraction from the shell in the corner due to the imposed flux drop, the immediate corner area still gets moderately cooled due to the 2D heat flow corner effect while the rest of the corner flux drop area stay warmest in the domain with as much as 120 C higher temperature than the rest of the domain and immediate corner. This is quantitatively very similar to the temperature corner profile from the previous 2D coupled simulations (Li, 2004, Koric, 2007).

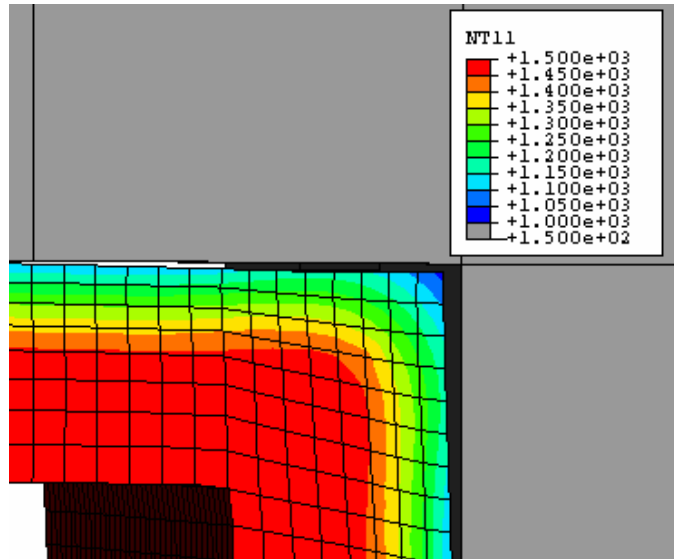


Figure 8. Detail corner bottom shell surface distortion with temperature contour at 12 sec.

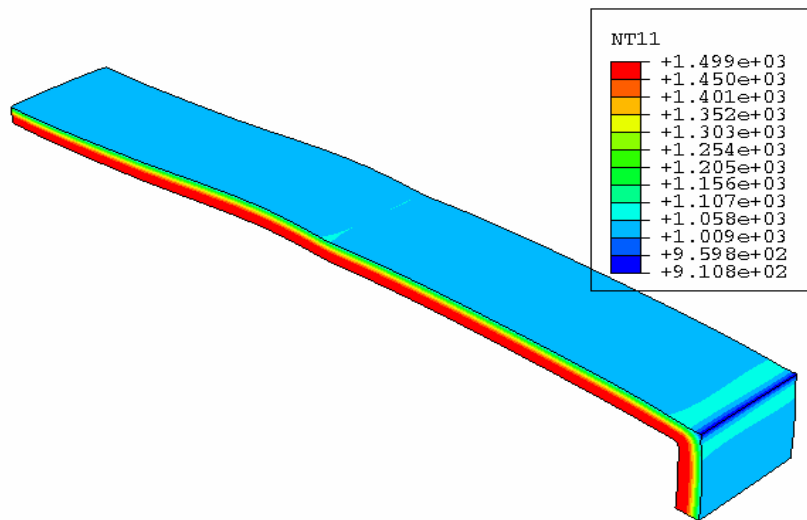


Figure 9. Temperature contour when domain bottom is 19 sec. below meniscus.

There are two major contributions to the generation of stress in this model. Besides usual thermo-viscoplastic stresses coming from solidification due to the uneven cooling through shell thickness, there is a strong pure mechanical component coming from the funnel geometry pushing and bending solidified shell. Often mechanical component is dominant in funnel region and stress sign is opposite of expected compression on shell surface and subsurface tension common for pure solidification of a straight shell. Most of the wide face, and especially in the funnel region, is in the state of tensile stress on the surface early as given in Fig. 10 depicting transverse stress contour σ_x at 5 sec. This can be explained by the significant deformation of the shell as it gets pushed by the funnel and straightened in the funnel region increasing its length. The shell transverse elongation is even larger than its corresponding shrinkage due to

the cooling, and the tension occurs on the shell surface. This is opposite of usual compression on the shell surface for the parallel molds without funnel.

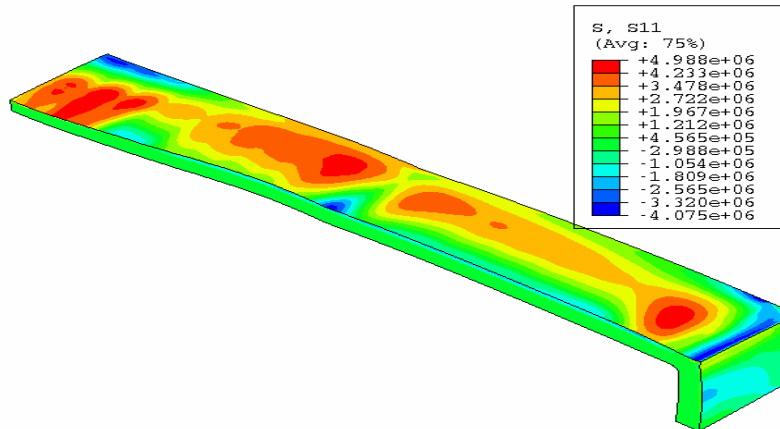


Figure 10. Transverse stress contour when domain bottom is 5 sec. below meniscus.

At later time of 12 sec. situation changes and most of wide face bottom edge is in compression except the funnel outer bend region that stays in the tensile state. Between 13.5 and 17 sec. most of the funnel shell surface goes into another period of tension, which is even stronger than at early times. That is the time when the shell in the funnel goes through the funnel mold wall transition region from the tapered to the straight. Finally, at the mold exit at 19 sec surface compression dominates everywhere again except in the small area around the center of the funnel where some residual tensile surface stress is still present. Generally subsurface stress lines are showing usual tensile stress close to solidification front when compression is on the surface, but opposite is also true for the most of the surface in tension.

Axial stress σ_z distribution and history are quantitatively similar to the transverse stresses and characterized again by the two stress reversals. At 5 sec high tensile stress areas are recorded close to symmetry planes, while in the corner area both tensile and compressive stresses are present next to each other due to the strong thermal strains coming from temperature corner variations. Most of shell surface is in compression due to its axial shrinkage at 12 sec except a tiny tensile strip at the corner edge. At the time of 15.8 sec. surface tension is present in most of the funnel region which is left from the axial unbending that shell undergoes after transition from tapered to straight part of the funnel mold wall, as given in Fig. 11. Finally at the mold exit, surface compression dominates again.

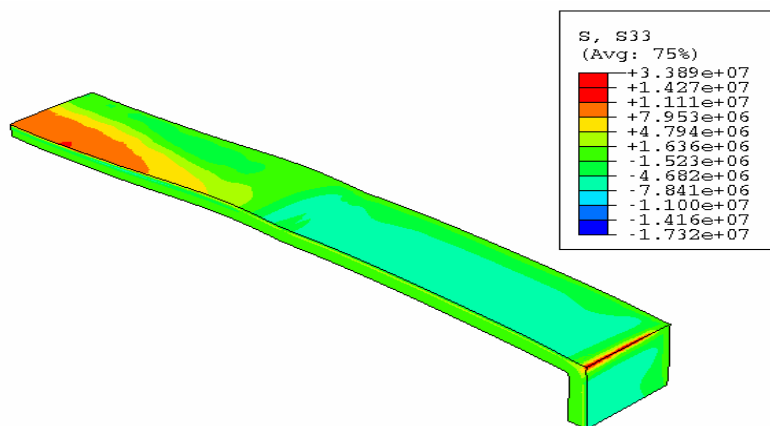


Figure 11. Axial stress contour when domain bottom is 15.8 sec. below meniscus.

Transverse and axial stress histories are given for the two interesting points on the bottom surface edge. Fig. 12 has stress histories for a center funnel point, and Fig. 13 has stress histories for a point 0.58 m from a center in a straight part of wide face. The stress histories for the funnel point is nicely depicting the two periods of stress reversals, while the straight part of funnel mostly behaves in an expected surface compression fashion observed from the validation model from the chapter 5.

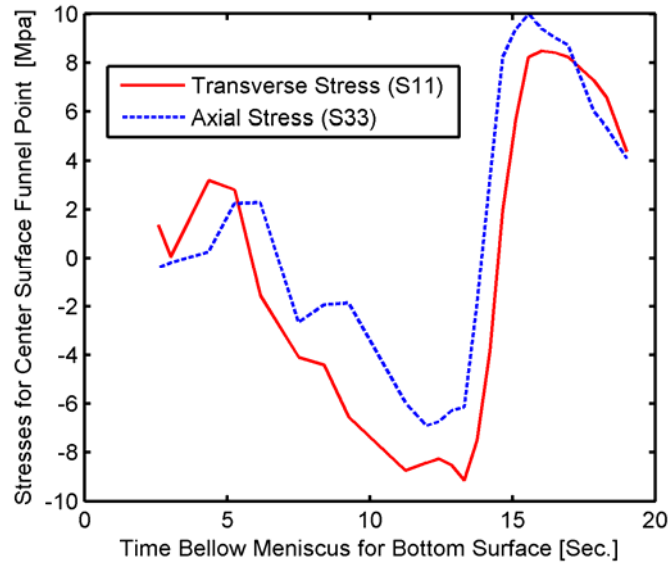


Figure 12. Stress histories for a center bottom surface wf point.

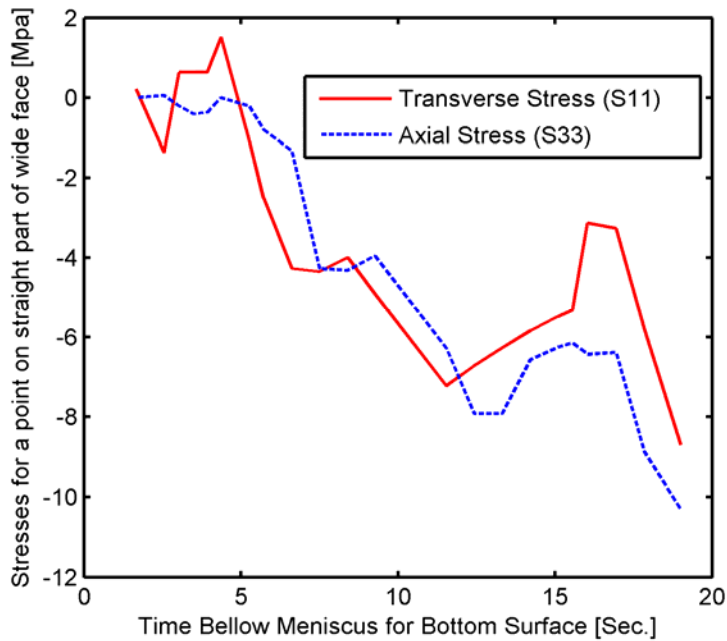


Figure 13. Stress histories for a bottom surface wf point, at the straight part

7. Conclusions

3D thermo-mechanical behavior of the strand in a thin funnel mold has been analyzed. The transient heat transfer analysis with realistic properties and heat flux boundary conditions was run first, followed by the mechanical analysis with 3D softened mechanical contact between the shell and the mold wall. This simulation provides the following insights into the continuous casting process for funnel thin slabs:

- This model indicates a significant interfacial gap develops at and near the corner, on the narrow face, owing to the lack of mold taper. Realistic mold taper data is necessary to be included in future models to compensate for the large gap formation.
- Large gradients of temperature are recorded between the corner tip and wider corner area. This is causing uneven shell development in the corner area, similar to beam blank casting (Koric, 2007), making the corner area prone to shell thinning, longitudinal cracks and other problems.
- Negligible temperature gradients are observed in the casting direction, justifying the assumption used in all 2D models that the heat conduction in axial (casting) direction can be neglected due to the large Peclet number.
- The strand surface is generally in compression, similar to the analytical solution. Two periods of stress reversals, characterized by the surface going into tension (and the subsurface into compression), are revealed for both transverse and axial shell stresses in the funnel area. The transverse stress reversals are consistent with the findings of Park et. al. (Park, 2002).
- The axial stress results are novel and can be used to predict internal transverse cracks. The results suggest that the sharp end of the funnel is responsible for the shell lifting off the mold wall, potentially leading to air gap formation, and cracking problems, in addition to the tensile stresses. Thus, the model suggests that moothing the transition from the funnel to the lower mold should alleviate this.
- Even though this pioneer attempt to model 3D solidification in a complex geometry environment of a thin slab continuous mold with funnel turned out to be a serious computational task, it clearly shows that the model developed in UMAT in previous work (Koric, 2006) is efficient enough to perform it successfully with Abaqus on the latest computational platforms.

8. References

1. Abaqus Inc., "User Manuals v6.5," Abaqus Inc., 2005
2. L. Anand., "Constitutive equations for the rate dependant deformation of metals at elevated temperatures," ASME Journal of Engineering Materials Technology, vol. 104, pp. 12-17, 1982
3. J.R. Boehmer, G. Funk, M. Jordan and F.N. Fett, "Strategies for coupled analysis of thermal strain history during continuous solidification processes," Advances in Engineering Software, vol. 29 (7-9) pp. 679-697, 1998
4. A. Cristallini, M. R. Ridolfi, A. Spaccarotella, R Caposti, G. Fleming and J. Sucker, "Advanced Process Modeling of CSP Design for Thin Slab Casting ," In 12th IAS Steelmaking Seminar, 1999
5. M.A. Crisfield, "Nonlinear FEA of Solids and Structures," Wiley, 1999
6. I. Farup and A. Mo, "Two-phase modeling of mushy zone parameters associated with hot tearing," Metall. Mater. Trans., vol. 31, pp. 1461-1472, 2000
7. A. Grill, J.K. Brimacombe, and F. Weinberg, "Mathematical analysis of stress in continuous casting of steel," Ironmaking Steelmaking, vol 3, pp. 38-47, 1976
8. S. Koric and B.G. Thomas, "Efficient Thermo-Mechanical Model for Solidification Processes," International Journal for Num. Methods in Eng., vol. 66, pp. 1955-1989, 2006
9. S. Koric, B. G. Thomas, K. Xu, and C. Spangler, "Coupled Thermo-Mechanical Model of Steel Beam Blanks: Part I Model Formulation and Validation", Metall. and Mat. Transactions (In Review), 2007
10. Kowaski Steel, Private Communications, 1996-1999
11. P.F. Kozlowski, B.G. Thomas, J.A. Azzi, and H. Wang., "Simple constitutive equations for steel at high temperature," Metallurgical Transactions, vol. 23A, pp. 903-918, 1992
12. J. O. Kristiansson, "Thermomechanical behavior of the solidifying shell within continuous casting billet molds-a numerical approach," Journal of Thermal Stresses, vol. 7, pp. 209-226, 1984

13. R.W. Lewis, K. Morgan, H.R.Thomas and KN.Seetharamu, "The Finite Element Method in Heat Transfer Analysis," Wiley New York, 1996
14. Chunsheng Li and B.G. Thomas, " Thermo-Mechanical Finite-Element Model of Shell Behaviour in Continuous Casting of Steel," *Metal and Material Trans. B*, vol. 35B(6), pp. 1151-1172, 2004
15. A.M. Lush, G. Weber and L. Anand, "An implicit time –integration procedure for a set of integral variable constitutive equations for isotropic elasto-viscoplasticity", *International Journal of Plasticity*, vol. 5, pp. 521-549, 1989
16. G.E. Mase and G. T. Mase. "Continuum mechanics for engineers," CRC Press Second Edition, 1999
17. A. Mendelson, "Plasticity: Theory and Applications," Krieger Pub. Co., 1983
18. H. Mizukama, S. Hiraki, M. Kawamoto and T. Watanbe, "Initial Solidification Behaviour of Ultra Low, Low, and Middle Carbon Steel," *ISIJ International*, vol 39, pp. 1262-1269, 1999
19. K. Morgan , R. W. Lewis, and J. R. Williams , "Thermal stress analysis of a novel continuous casting process," *The Mathematics of Finite Elements and its Applications* Academic Press, vol. 3, 1978
20. Joong Kil Park, Brian G. Thomas, and Indira Samarasekera, "Analysis of Thermo-Mechanical Behavior in Thin Slab Casting," Internal Report University of British Columbia, 2002
21. F.G Rammerstrofer, C. Jaquemar, D.F. Fischer, and H. Wiesinger, "Temperature fields, solidification progress and stress development in the strand during a continuous casting process of steel," *Numerical Methods in Thermal Problems*, Pineridge Press, pp 712-722, 1979
22. J.M. Risso, A.E. Huespe, and A. Cardona, "Thermal stress evaluation in the steel continuous casting process," *International Journal for Numerical Methods in Engineering*, vol. 65(9), pp. 1355-1377, 2006
23. Thomas, B. G., J. K. Brimacombe, and I. V. Samarasekera, "The Formation of Panel Cracks in Steel Ingots, A State of the Art Review, Hot Ductility of Steel," *Trans. of the Iron and Steel Society*, Vol. 7, pp. 7-20, 1986
24. J.H. Weiner and B.A. Boley, "Elastic-plastic thermal stresses in a solidifying body," *J. Mech. Phys. Solids*, vol. 11, pp. 145-154, 1963
25. F. Wimmer, H. Thone, and B. Lindorfer, "Thermomechanically-coupled analysis of the steel solidification process in continuous casting mold," , Abaqus Users Conference, 1996
26. O.C. Zienkiewicz and R.L. Taylor, " Finite element method: solid and fluid mechanics dynamics and non-linearity", McGraw-Hill, 1991
27. H. Zhu, " Coupled thermal-mechanical finite-element model with application to initial solidification. ", Ph.D. Thesis, University of Illinois, 1993

Acknowledgement

The authors would like to thank the National Center for Supercomputing Applications (NCSA) at the University of Illinois for providing computing facilities.